Compatibility in Microstructural Optimization for Additive Manufacturing

Eric Garner[a], Helena M.A. Kolken[b], Charlie C.L. Wang[a], Amir A. Zadpoor[b], Jun Wu[a]

[a]*Department of Design Engineering, TU Delft, The Netherlands*
[b]*Additive Manufacturing Laboratory, Department of Biomechanical Engineering, TU Delft, The Netherlands*

Abstract

Microstructures with spatially-varying properties such as trabecular bone are widely seen in nature. These functionally graded materials possess smoothly changing microstructural topologies that enable excellent micro and macroscale performance. The fabrication of such microstructural materials is now enabled by additive manufacturing (AM). A challenging aspect in the computational design of such materials is ensuring compatibility between adjacent microstructures. Existing works address this problem by ensuring geometric connectivity between adjacent microstructural unit cells. In this paper, we aim to find the optimal connectivity between topology optimized microstructures. Recognizing the fact that the optimality of connectivity can be evaluated by the resulting physical properties of the assemblies, we propose to consider the assembly of adjacent cells together with the optimization of individual cells. In particular, our method simultaneously optimizes the physical properties of the individual cells as well as those of neighbouring pairs, to ensure material connectivity and smoothly varying physical properties. We demonstrate the application of our method in the design of functionally graded materials for implant design (including an implant prototype made by AM), and in the multiscale optimization of structures.

Keywords: Topology optimization, Inverse homogenization, Functionally graded materials, Multiscale optimization, Compatible microstructures

1. Introduction

In recent years, advances in additive manufacturing have made it possible to fabricate cellular materials whose mechanical properties are defined not only by their chemical composition, but also by their microscale topologies [1]. These microstructural materials, also referred to as architected materials [2] or meta-materials [3], can be designed to possess highly tailored or extreme physical properties not usually found in nature.

A systematic approach in the computational design of microstructural materials is to define the material as a periodic array of identical unit cells, and to formulate it as a topology optimization problem [4]. This process, often called inverse homogenization [5], optimizes the material distribution within the design space of a single unit cell, and uses homogenization theory to evaluate the effective properties of the material. Inverse homogenization has been used to design periodic microstructures with exceptional properties such as maximized bulk modulus [5, 6], negative Poisson's ratio [5, 7], and negative thermal expansion [8], among others (cf. [9, 2]).

While the optimization of periodic microstructures has been studied in depth, less attention has been paid to the assembly of optimized microstructures with spatially-varying properties. Such inhomogeneous microstructures are of great importance in engineering design. For instance, when designing orthopaedic implants, it may be desirable to have a continuous transition from denser microstructures in the central region to highly porous microstructures at the bone-implant interface. This functional gradation promotes bony ingrowth at the bone-implant interface, while maintaining structural integrity and increasing the mechanical properties in the areas where bony ingrowth is irrelevant [10].

Figure 1: Illustration of poorly connected microstructures. The unit cells are individually optimized for maximum bulk modulus under linearly-varying volume fractions from 30% to 50%, from left to right.

A critical issue in the assembly of spatially-varying microstructures relates to the compatibility of neighbouring microstructures. As illustrated in Fig. 1, individually optimized neighbouring cells do not necessarily form an integral part, and the physical properties along their shared boundaries are unpredictable and often inferior to those of the individual microstructures.

Existing works typically address this problem by pursuing geometric connectivity between adjacent microstructural unit cells. In the design of functionally graded materials (FGMs), Zhou and Li [11] proposed three methods to address the connectivity issue, namely *kinematic connective constraint*, *pseudo load* and *unified formulation with non-linear diffusion*. In the first two methods, unit cells are optimized individually, while

*Corresponding author
Email address: j.wu-1@tudelft.nl (Jun Wu)

constraints are imposed to connect optimized cells with predefined common regions. The kinematic approach has been adopted by Li et al. [12]. In the unified formulation, unit cells are optimized all together, and a non-linear diffusion term is introduced in the objective function to penalize disconnection. The computational efficiency of the unified formulation is improved by successively optimizing new unit cells while considering connection to cells that have been optimized [13]. An alternative approach is to optimize some key microstructures, and apply geometric interpolation to obtain intermediate microstructures between individually optimized unit cells [14]. This geometric approach works for microstructures of similar topology.

In this paper, we aim to find the optimal connectivity between topology optimized microstructures. Given the fact that the optimality of connectivity can be evaluated by the resulting physical properties of the assemblies, we propose to consider the assembly of adjacent cells together with the optimization of individual cells. In particular, our method simultaneously optimizes the physical properties of the individual cells as well as those of neighbouring pairs, to ensure material connectivity and smoothly varying physical properties. This idea is substantiated on the design of graded microstructures with maximized bulk moduli under varying volume fractions. The graded microstructures are employed in designing an implant (cf. Fig. 2), which is fabricated by additive manufacturing.

Our method could also be applied to improve multiscale structural optimization, where poor connectivity across neighbouring microstructures has recently received considerable attention. For example, Cramer et al. [14] proposed a bottom-up approach to multiscale optimization, where a set of optimized and interpolated microstructures is used as building blocks for macroscale optimization. To circumvent the connectivity issue in optimized microstructures, parametrized lattice structures are commonly used in bottom-up approaches (e.g. [15, 16, 17]). The parametrization, nevertheless, reduces the design space and limits the range of possible topologies. Our method places no restrictions on the topology and generates optimized, compatible microstructures. In a different approach, Zhu et al. [18] proposed a two-scale method where the gamut of microstructures is precomputed. In the subsequent mapping process, boundary similarity across adjacent cell interfaces is taken into account for selecting the microstructures.

Concurrently optimizing the microstructural material and the macrostructure gives more flexibility in design. Rodrigues et al. [19] proposed hierarchical optimization of material and structure. This was later extended to 3D [20]. Integrating our method into the hierarchical approach results in two-scale structures with improved connectivity. A recent survey on hierarchical optimization of material and structure is given by Xia and Breitkopf [21]. In contrast to the isoparametric microstructures with four-fold rotational symmetry generated in the design of FGMs, the microstructures generated in concurrent multiscale optimization possess two-fold rotational symmetry and therefore more topological variations and direction-dependent properties. Wang and colleagues [22, 23] developed a level-set method to obtain topologically similar and, thus, connectable, microstructures. Du and Kim [24] proposed a physics-independent connectivity index, which ensures good geometric connectivity by progressively modifying each microstructure to be well connected to its nearest neighbour. Alexandersen and Lazarov [25] and Wu et al.[26, 27] performed structural analysis and optimization on the fully refined microstructure details, naturally ensuring the connectivity of the resulting microstructures. The full scale analysis is computationally intensive, thereby limiting the microstructural details that can be practically optimized.

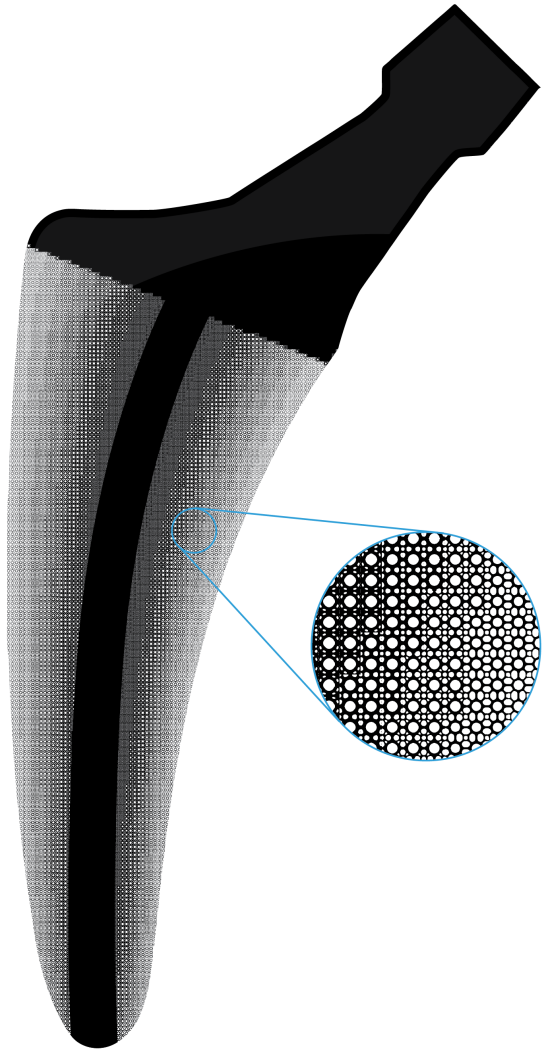

Figure 2: An orthopaedic implant with functionally graded microstructures optimized by the proposed method. The different microstructures have distinct topologies but are still well connected, forming an integral part.

The remainder of the paper is organized as follows. In Section 2, we introduce the compound formulation for optimizing compatibility in microstructures, building upon inverse homogenization and density-based topology optimization. In Section 3, we analyze the performance of optimized microstructures and demonstrate their usage in the design of an implant. Section 4 demonstrates the applicability of the proposed method in multiscale structure optimization. Finally, the most important conclusions from this study are summarized in Sec-

tion 5.

2. Compatibility Optimization with Compound Formulation

To start with, let us consider the design of a 2D functionally graded cellular material with a density gradation in one direction and periodicity in the other (see Fig. 3). The design domain of the graded material (referred to as GM) is composed of N square subdomains, each for a unique unit cell. Generating the unit cells in isolation leads to the lack of connectivity between adjacent cells. Here, we propose a holistic approach that generates the unit cells simultaneously in a unified formulation, incorporating the mechanical behaviour across adjacent microstructures in the optimization.

The design of graded materials is formulated as an inverse homogenization problem based on finite element analysis and density-based topology optimization [28]. Let us denote the design domain of the GM by Ω and the subdomain of each unit cell by $\Omega^n, n = 1, ..., N$. Each subdomain is discretized into square finite elements for mechanical analysis. For each element, the volume fraction of solid material (also referred to as pseudo density), $\rho_e^n \in [0, 1]$, serves as the design variable, with $\rho_e^n = 0$ (or $\rho_e^n = 1$) indicating that the element is empty (or solid). The density distribution within each unit cell is optimized to maximize a specific mechanical property (e.g. bulk modulus), derived from the effective elasticity tensor, and is subject to a volume fraction constraint, which varies linearly in the graded direction.

To ensure optimal connectivity between adjacent cells, the idea is to directly incorporate into the objective function a term which quantifies the degree of connectivity. A simple measure of connectivity between adjacent cells is the number of shared elements across the interface. This type of geometric measures, however, does not reflect any mechanical properties of the connection. An effective and intuitive measure of the mechanical connectivity considers the mechanical properties of the assembled cells as a compound part. To this end, we introduce the concept of compound cells. Each compound cell is composed of two neighbouring unit cells (Fig. 4). The mechanical properties of the compound cell serve as an effective measure of the mechanical connectivity. The objective function is therefore defined as a weighted average of the individual and compound cell objectives.

The mathematical formulation of the optimization problem is written as

$$\begin{aligned} \max_{\rho} \quad & J = (1-\omega)\sum_{n=1}^{N} f(E^H(\boldsymbol{\rho}^n)) + \\ & \qquad \omega \sum_{n=1}^{N-1} f(E^H([\boldsymbol{\rho}^n, \boldsymbol{\rho}^{n+1}])) \\ \text{s.t.} \quad & : \sum_{e=1}^{M} v_e^n \rho_e^n / |Y^n| \le V^n, \ \forall n \\ & : 0 \le \rho_e^n \le 1, \ \forall e, n. \end{aligned} \tag{1}$$

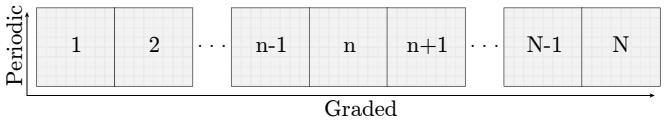

Figure 3: Illustration of a 2D graded material, comprising N unique unit cells.

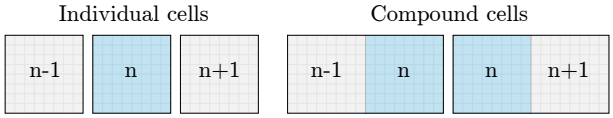

Figure 4: Unit cell n shown individually and a part of compound cells $(n-1, n)$ and $(n, n+1)$.

In the objective function, an abstract function f derives an objective from the effective elasticity tensor (E^H), which depends on the density vector $\boldsymbol{\rho}^n$ (or $[\boldsymbol{\rho}^n, \boldsymbol{\rho}^{n+1}]$) of a unit (or compound) cell. A weighting factor ω determines the influence of the compound cells on the optimization of individual unit cells. With $\omega = 0$, this objective function is equivalent to the microstructure design formulation where the connectivity is not taken into account.

The first constraint restricts the volume fraction of each individual cell. M is the number of the finite elements per unit cell. v_e^n is the area or volume of a finite element. $|Y^n|$ is the area or volume of the unit cell domain. V^n is a prescribed volume fraction. The second constraint restricts the element density ρ_e^n between 0 and 1. For the sake of clarity, the state equations which are known in inverse homogenization for evaluating the elasticity tensor (E^H) are omitted here, and will be introduced in the following subsection.

This formulation can be extended to achieve some desirable properties of the graded material, e.g., gradation in multiple directions. The optimization problem as formulated in Eq. 1 only ensures that neighbouring unit cells are compatible along a single direction. The compatibility along the other direction can be ensured by a rotational symmetry constraint on each unit cell. This constraint has been realized by assigning a single design variable to, and averaging the sensitivities of, the elements that are corresponding due to the symmetry condition [29].

More extensions will be discussed and their effects on the optimized cells will be demonstrated in the results section. In the following, we proceed to the essential steps in inverse homogenization.

2.1. Homogenization

We make use of homogenization theory to predict the effective elasticity tensor of both individual and compound cells. According to the homogenization theory [30, 5, 31], the effective elasticity tensor (E^H) for a periodic microstructure is given by

$$E_{ijkl}^H = \frac{1}{|Y|}\int_Y E_{ijpq}(\varepsilon_{pq}^{0(kl)} - \varepsilon_{pq}^{*(kl)})dY, \tag{2}$$

where $|Y|$ is the area or volume of the cell domain Y in $\mathbb{R}^2$ or $\mathbb{R}^3$, respectively. $\varepsilon_{pq}^{0(kl)}$ corresponds to the independent unit test

strains (in 2D there are three; e.g. unit strain in the horizontal direction, unit strain in the vertical direction, and unit shear strain). $\varepsilon^{*(kl)}_{pq}$ is the Y-periodic solution to the variational type problem

$$\int_Y E_{ijpq}\varepsilon^{*(kl)}_{pq}\frac{\partial \nu_i}{\partial y_i}dY = \int_Y E_{ijpq}\varepsilon^{0(kl)}_{pq}\frac{\partial \nu_i}{\partial y_i}dY,\ \forall \nu \in V, \quad (3)$$

where ν is a Y-admissible displacement field.

Using an energy-based approach [32], the elasticity tensor is rewritten as

$$E^H_{ijkl} = \frac{1}{|Y|}\int_Y E_{pqrs}\Big(\varepsilon^{0(ij)}_{pq} - \varepsilon^{*(ij)}_{pq}\Big)\Big(\varepsilon^{0(kl)}_{rs} - \varepsilon^{*(kl)}_{rs}\Big)dY. \quad (4)$$

In finite element form, for a cell discretized into M elements, the effective tensor is approximated by

$$E^H_{ijkl} = \frac{1}{|Y|}\sum_{e=1}^{M}(\mathbf{u}^{*(ij)}_e)^T\mathbf{k}_e\mathbf{u}^{*(kl)}_e, \quad (5)$$

where $\mathbf{u}^{*(ij)}_e$ are the element displacement solutions corresponding to the unit test strain fields $\varepsilon^{0(ij)}$, and $\mathbf{k}_e$ is the stiffness matrix of an element.

It should be noted that the homogenization theory assumes infinite periodicity of the microstructures, and as such may not provide accurate results when used to generate spatially-varying microstructure distributions. However, it has been shown that reasonable accuracy can be expected if the gradient of material properties is sufficiently small [11]. This has been confirmed in our numerical tests.

2.1.1. Equilibrium equations

To evaluate the elasticity tensor, equilibrium equations corresponding to the linearly independent unit test strain fields must be solved for each individual and compound cell. For the individual cells, the equilibrium is written as:

$$\mathbf{K}_n\mathbf{U}^{A(kl)}_n = \mathbf{F}^{(kl)}_n,\ k,l = 1,...,d,\ n = 1,...,N, \quad (6)$$

and for the compound cells:

$$\mathbf{K}_{n,n+1}\mathbf{U}^{A(kl)}_{n,n+1} = \mathbf{F}^{(kl)}_{n,n+1},\ k,l = 1,...,d,\ n = 1,...,N-1, \quad (7)$$

where, for each individual cell n, $\mathbf{K}_n$ is the global stiffness matrix, $\mathbf{U}^{A(kl)}_n$ and $\mathbf{F}^{(kl)}_n$ are the global displacement vector and external force vector of the test case (kl), respectively. Similarly, for each compound cell $(n, n+1)$, $\mathbf{K}_{n,n+1}$ is the global stiffness matrix, $\mathbf{U}^{A(kl)}_{n,n+1}$ and $\mathbf{F}^{(kl)}_{n,n+1}$ are the global displacement vector and external force vector of the test case (kl), respectively.

The individual contributions of each element to the global stiffness matrix $\mathbf{K}_n$ are calculated as $\mathbf{k}_e = E_e(\rho_e)\mathbf{k}_0$, where $\mathbf{k}_0$ is the stiffness matrix of a solid element and $E_e(\rho_e)$ is the Young's modulus corresponding to element e, interpolated via the modified solid isotropic material with penalization (SIMP), given by

$$E_e(\rho_e) = E_{min} + \rho^\gamma_e(E_0 - E_{min}), \quad (8)$$

where E_0 is the Young's modulus of a solid element, E_{min} is a small term assigned to prevent the global stiffness matrix from becoming singular, and γ is a penalization factor (typically $\gamma = 3$).

2.1.2. Objective function

The objective function is formulated to maximize or minimize a specific material property, derived from the elasticity tensor. Using the engineering notation with $11 \to 1$, $22 \to 2$, and $12 \to 3$, the elasticity tensor, E^H_{ijkl} in Eq. (5), is rewritten as

$$G_{ij} = \frac{1}{|Y|}\sum_{e=1}^{M}(\mathbf{u}^{*(i)}_e)^T\mathbf{k}_e\mathbf{u}^{*(j)}_e. \quad (9)$$

For the individual and compound cells, respectively, the objective is defined generically as:

$$f(\overline{G}(\boldsymbol{\rho}^n)) = \sum_{i,j=1}^{3} r_{ij}G^n_{ij}, \quad (10)$$

and

$$f(\overline{G}([\boldsymbol{\rho}^n, \boldsymbol{\rho}^{n+1}])) = \sum_{i,j=1}^{3} r_{ij}G^{n,n+1}_{ij}, \quad (11)$$

where r_{ij} are constant values, typically 1 or 0. For maximizing bulk modulus, $r_{11} = r_{22} = r_{12} = r_{21} = 1$, all others are 0. $G^{n,n+1}_{ij}$ represents the elasticity tensor of the compound cell composed of unit cells n and $n+1$.

The optimization problem is solved by the method of moving asymptotes (MMA) [33]. The required sensitivities for the objective functions (10) and (11) are, respectively

$$\frac{\partial f}{\partial \rho}\Big(\overline{G}(\boldsymbol{\rho}^n)\Big) = \sum_{i,j=1}^{3} r_{ij}\frac{\partial G^n_{ij}}{\partial \rho}, \quad (12)$$

and

$$\frac{\partial f}{\partial \rho}\Big(\overline{G}([\boldsymbol{\rho}^n, \boldsymbol{\rho}^{n+1}])\Big) = \sum_{i,j=1}^{3} r_{ij}\frac{\partial G^{n,n+1}_{ij}}{\partial \rho}, \quad (13)$$

where $\frac{\partial G^n_{ij}}{\partial \rho}$ and $\frac{\partial G^{n,n+1}_{ij}}{\partial \rho}$ are computed using the adjoint method [4]

$$\frac{\partial G_{ij}}{\partial \rho} = \frac{1}{|Y|}\gamma\rho^{\gamma-1}_e(E_0 - E_{min})(\mathbf{u}^{*(i)}_e)^T\mathbf{k}_0\mathbf{u}^{*(j)}_e. \quad (14)$$

2.2. Three-field SIMP

We make use of the three-field approach in topology optimization using SIMP [34, 35, 36]. Rather than directly optimizing the density field ρ, a design field ϕ is introduced. The design field ϕ is smoothed by a density filter, obtaining a smoothed field $\tilde{\phi}$. This is followed by a projection operation using a smoothed Heaviside function to obtain the density field $\rho = \overline{\tilde{\phi}}$.

2.2.1. Filtering

The density filter eliminates common checkerboard (i.e., regions of alternating solid and void elements) inherent to low order discretization. The smoothed density $\tilde{\phi}_e$ is defined as a weighted average of the neighbouring design variables, i.e.,

$$\tilde{\phi}_e = \frac{\sum_{i\in\mathbb{M}_e}\omega_{i,e}\phi_i}{\sum_{i\in\mathbb{M}_e}\omega_{i,e}}, \quad (15)$$

where the neighbourhood of element e is defined as

$$\mathbb{M}_e = \{i | \, \|x_i - x_e\|_2 \leq r_e\}, \tag{16}$$

where r_e is the filter radius and the weighting factor $\omega_{i,e}$ depends linearly on the distance between elements, i.e.,

$$\omega_{i,e} = 1 - \frac{\|x_i - x_e\|_2}{r_e}. \tag{17}$$

The density filter is applied over the ordered sequence of unit cells in the GM, rather than within individual unit cells. This strategy has been used by Radman et al. [13]. This global filtering has the effect of reducing sharp features, and thus promotes smooth transitions at the boundaries between adjacent unit cells.

2.2.2. Projection

To ensure convergence to a binary (i.e. solid and void) solution, we use the parametrized projection function. The projected physical density is

$$\rho = \bar{\tilde{\phi}}_e = \frac{\tanh(\beta\eta) + \tanh(\beta(\tilde{\phi}_e - \eta))}{\tanh(\beta\eta) + \tanh(\beta(1-\eta)}. \tag{18}$$

The parameter β controls the sharpness of the threshold function. To avoid instability, we use a parameter continuation starting with $\beta = 1$ and double its value every certain number of iterations. The parameter η is the projection threshold. Following the robust formulation proposed by Wang et al. [37], dilated ρ^d, intermediate ρ^i and eroded ρ^e designs are formulated using thresholds η, 0.5, and $(1-\eta)$, with $\eta = 0.25$. This enforces a minimum length scale on both solid and void phases.

3. Results and Analysis

The proposed method has been implemented in Matlab based on the code developed by Xia and Breitkopf [31]. In this section, we present and analyze the results.

3.1. 2D functionally graded materials (FGM)

A 2D FGM is optimized for maximum bulk modulus with linearly-varying volume fraction from 30% to 80%. The domain is discretized into 8 unique microstructures, each with 200×200 elements. Fig. 5 a) and b) compare results without ($\omega = 0$) and with compound formulation ($\omega = 1$).

The results confirm that the compound formulation ensures material connectivity between adjacent microstructures, particularly between the first and second and between the third and fourth cells, which are otherwise poorly connected. Moreover, the material transitions between adjacent cells are very smooth despite each microstructure exhibiting remarkably different topologies from one to another.

To assess the mechanical compatibility between adjacent structures, the bulk modulus for each individual and compound cell is plotted in Fig. 6, together with the theoretical Hashin-Shrickman (HS) upper bounds [38]. Several observations can be made from the results of the compound formulation. Firstly, the performance of the individual cells agrees well with the HS bounds, meaning that the optimization of connectivity does not compromise the optimality of individual cells. This can be attributed to the large design space in topology optimization. Secondly, the performance of compound cells is close to the theoretical limit. This contrasts the performance of those obtained via the reference formulation ($\omega = 0$), which are frequently inferior to those of either of their constituent microstructures.

3.2. FGM with maximum length scale

The formulation can be extended to allow control over the maximum length scale on the design. Together with the minimum length scale, this can reduce the variation in the thickness of the microstructures. We make use of the local volume constraint [26] to (approximately) control the maximum length scale. The constraint is formulated as:

$$\hat{\rho}_e \leq \alpha, \ \forall e, \tag{19}$$

where α is the prescribed upper bound on $\hat{\rho}_e$, which is the average element density in a neighbourhood $\mathbb{N}$ surrounding e, i.e.,

$$\hat{\rho}_e = \frac{\sum_{i \in \mathbb{N}_e} \rho_i}{\sum_{i \in \mathbb{N}_e} 1}. \tag{20}$$

The neighbourhood $\mathbb{N}_e$ is defined as the set of elements within an influence radius R_e of element e, i.e.,

$$\mathbb{N}_e = \{i | \, \|x_i - x_e\|_2 \leq R_e\}. \tag{21}$$

Figure 5 c) shows the effects of a maximum length-scale constraint. Here, besides prescribing a global volume fraction for each microstructure, a local volume bound ($\alpha = 95\%$) is also used. This constraint enriches the topology especially in the unit cells with a high volume fraction. The connectivity between unit cells of distinct topologies can be observed.

The bulk moduli of individual and compound cells optimized with and without a maximum length scale are plotted in Fig. 7. It can be observed that the bulk moduli in both settings agree well with the HS bounds. To the right of the plot (i.e., microstructures with high material volume fractions), the cells optimized with this local constraint have a smaller global volume fraction than those without this constraint. This is due to the fact that local volume constraints are more restrictive. Similar effects have been reported in a study where local volume constraints were originally proposed for compliance minimization [26].

3.3. FGM for orthopaedic implant design

FGMs are extremely useful in the design of mechanical components with spatially-varying requirements. We apply the compound formulation to the design of an orthopaedic hip implant with high porosity on the bone-implant interface and high density in the core region. We include an isotropy constraint in the form of a cubic-symmetry constraint and an additional constraint on the stiffness tensor:

$$G_{11} + G_{22} - (G_{12} + G_{21}) - 4G_{33} = 0. \tag{22}$$

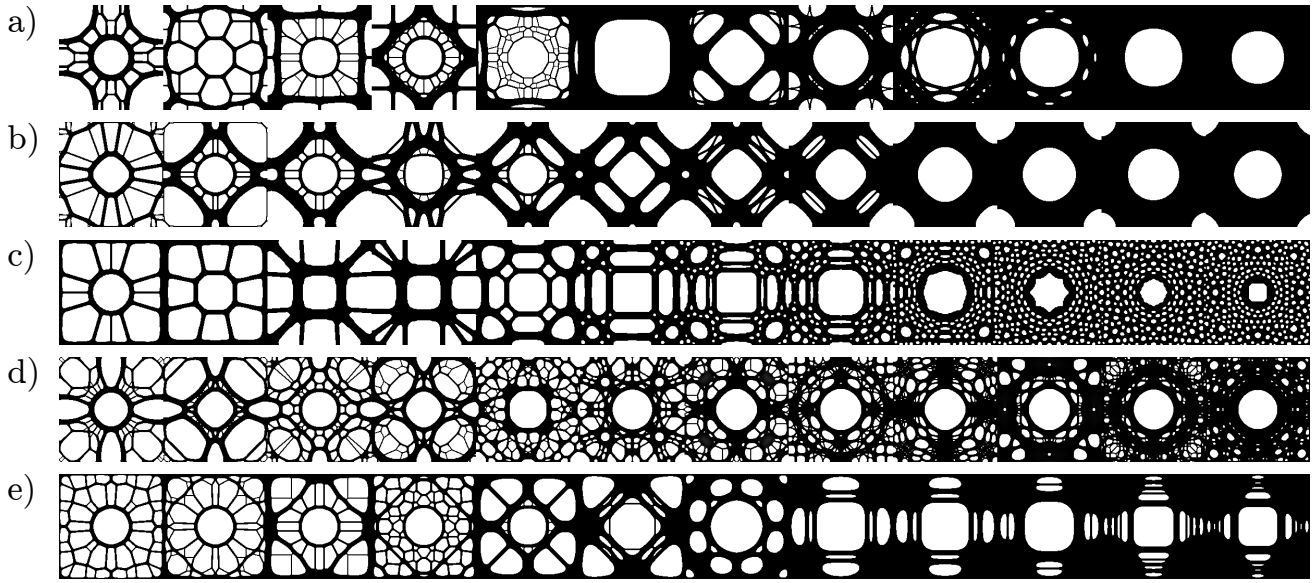

Figure 5: 2D FGMs optimized for maximum bulk modulus under linearly-varying volume fraction from 30% to 80% a) with $\omega = 0$; b) with $\omega = 1$; c) with local volume constraint ($\alpha = 95\%$, $R_e = 10$); d) with additional isotropy constraint; e) with mutual compatibility.

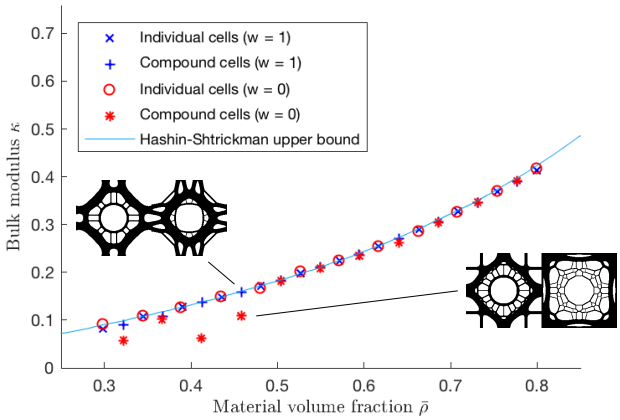

Figure 6: Bulk modulus vs. material volume fraction for FGM generated with ($\omega = 1$) and without ($\omega = 0$) compound formulation.

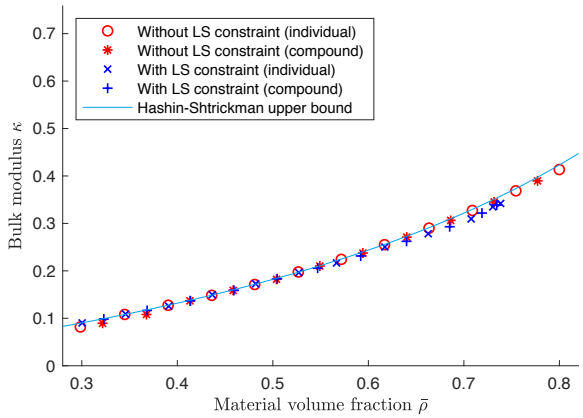

Figure 7: Bulk modulus vs. material volume fraction for the optimized FGM with/without a maximum length scale (LS).

The isotropy constraint is included to reduce the sensitivity of the structure to loading conditions . The effects of the isotropy constraint are shown in Fig. 5 d). We also introduce a local volume constraint ($\alpha = 95\%, R_e = 10$), which limits the size of solid material regions, thus increasing the number and size of pores necessary for dendritic bone ingrowth.

We first optimize a set of 9 microstructures for maximum bulk modulus under linearly-varying volume constraint from 40% to 90%. Each cell is discretized into 100×100 finite elements. We then map the optimized microstructures into the implant to obtain the desired functional gradation. The process and final geometry are shown in Fig. 8. The 2D microstructures are extruded to obtain a 3D model. Fig. 9 shows a titanium specimen fabricated via selective laser melting.

A similar methodology can be applied to the design of infill patterns for 3D printing where spatially-varying structural requirements exist. In this case, the density distribution can be user-defined or determined based on the stress distribution. We then optimize a family of microstructures for maximum bulk modulus in a specific range of volume fraction and map them into the structure in the same way as for the orthopaedic implant.

3.4. Granularity

When mapping microstructures into a macrostructure for both FGM design and bottom-up multiscale optimization (to be introduced in the next section), the discretization of a continuous density distribution introduces some error that is inversely correlated to the granularity of the discretization. It is therefore useful to be able to generate large families of microstructures. However, the computational effort required to simultaneously

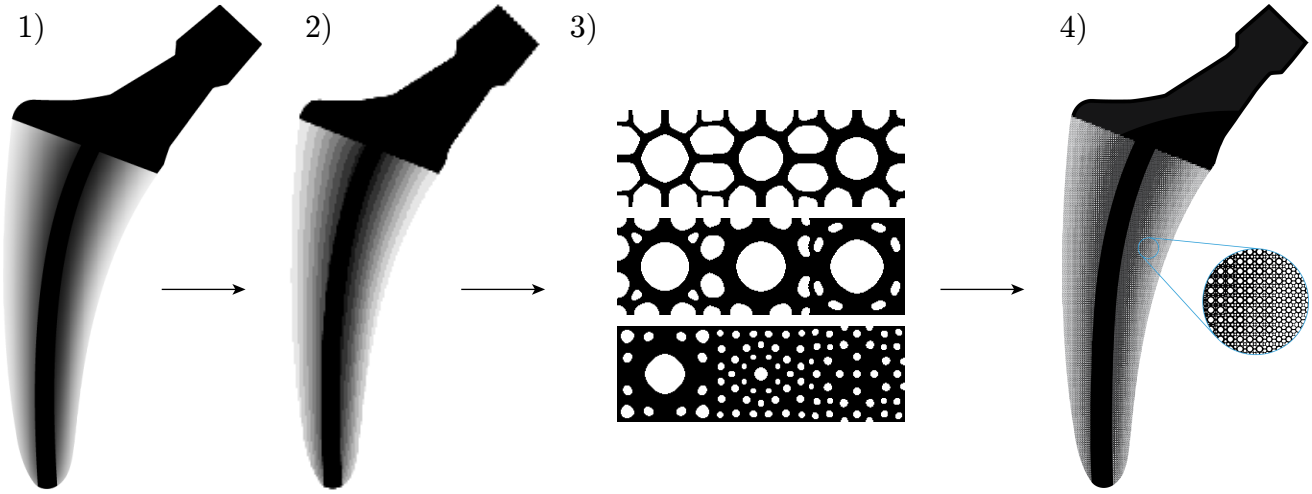

Figure 8: Implant development: 1) Define density distribution; 2) Discretize distribution; 3) Generate compatible microstructures; 4) Map microstructures into discretized density distribution.

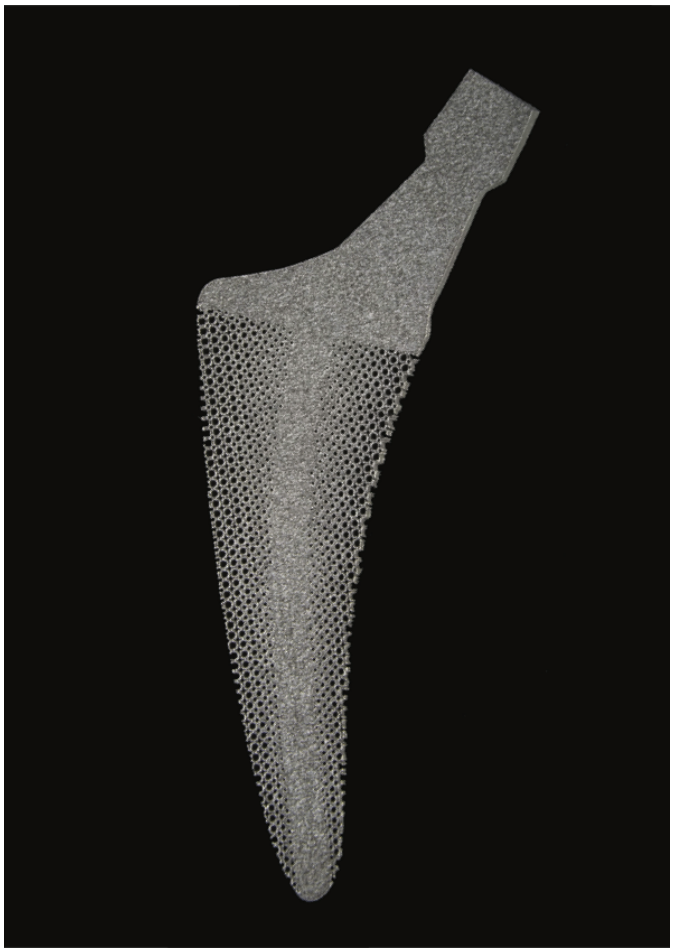

Figure 9: A specimen fabricated using selective laser melting (SLM). Material: Ti-6Al-4V ELI ASTM B348 with a particle size range of 10-45 micron. Machine: Realizer SLM125, Additive Manufacturing Laboratory, TU Delft.

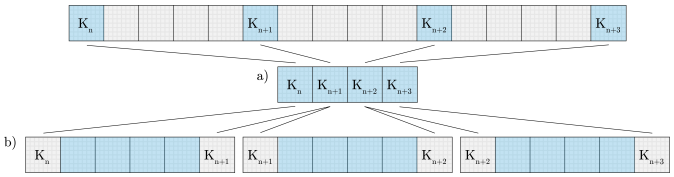

Figure 10: Interpolated GM optimization scheme. a) Key unit cells are optimized as a reduced GM. b) Intermediate unit cells are optimized as GMs with fixed key unit cells at either ends.

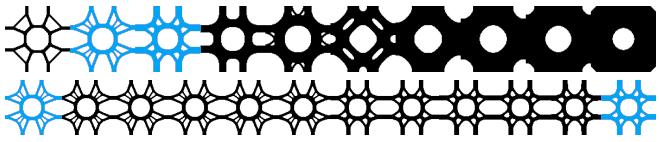

Figure 11: Key cell family (top) and interpolated cell family belonging to key cells two and three (bottom).

design a large number of unit cells may become problematic. Instead, an interpolation method can be used to break-up the problem into a series of more manageable ones. Firstly, a reduced set of uniformly distributed key unit cells is optimized. Subsequently, the intermediate unit cells between the key cells are optimized as smaller GMs with key cells set as fixed bounds and using the key cells as an initial guess. Fig. 10 depicts the process graphically. A set of interpolated cells is shown in Fig. 11. As a reference, we also optimized the full granularity of 100 cells simultaneously. Fig. 12 compares the bulk modulus on the interpolated cells as depicted in Fig. 11. The bulk modulus of the interpolated cells is very close to that of the full-granularity optimized cells. For cells with low volume fraction, the difference in modulus is relatively large, but still less than 5%.

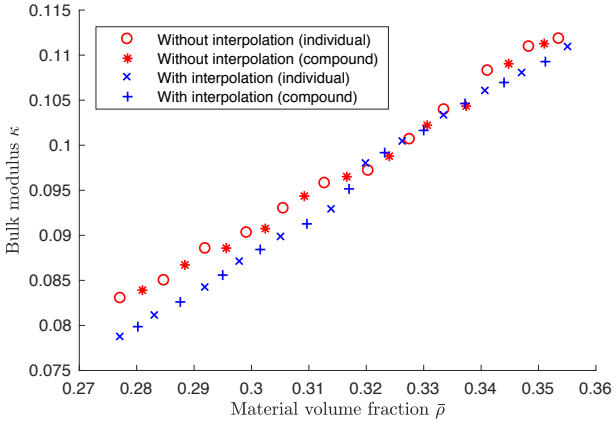

Figure 12: Bulk modulus vs. material volume fraction for cells optimized with and without the interpolation method.

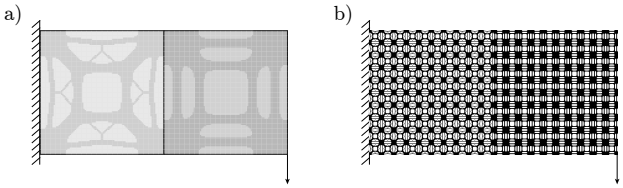

Figure 13: Cantilevered beam with two microstructural regions (50% and 60%): a) with homogenized properties assigned to each macroscale element; b) full-scale structure with $m \times m$ microstructural unit cells for each macroscale element.

3.5. Full-scale analysis

Homogenization theory assumes the separation of scales [30]. In engineering however it is impractical to fabricate an infinite array of periodic microstructures. This leads to an unavoidable discrepancy in structural performance between homogenization-based analysis and a full-scale analysis on the non-infinite array of microstructures. To investigate this discrepancy, we set up a cantilevered beam made up of two microstructural regions, as shown in Fig. 13. Each microstructural region is discretized with $m \times m$ elements. In Fig. 13 a) each element is assigned with the homogenized properties, while in Fig. 13 b) each element is realized by the microstructural unit cell. Fig. 14 plots the normalized compliance regarding the resolution of the microstructural array. The normalized compliance is defined as the compliance obtained with homogenized properties over the compliance of the full-scale structure. As the resolution increases, the normalized compliance approaches 1. The error is within 5% with microstructural resolutions as low as 18×18. In this example the two regions have a large difference (10%) in material fraction. This error becomes small as the difference in material fraction decreases. The full-scale analysis is performed using a multigrid-CG solver [39].

We compare this discrepancy with microstructures optimized without consideration for compatibility. The numbers are reported in Table 1. A resolution of 10×10 is used for both types of microstructures. It is observed that the compliance of a full-scale structure made up of incompatible microstructures is

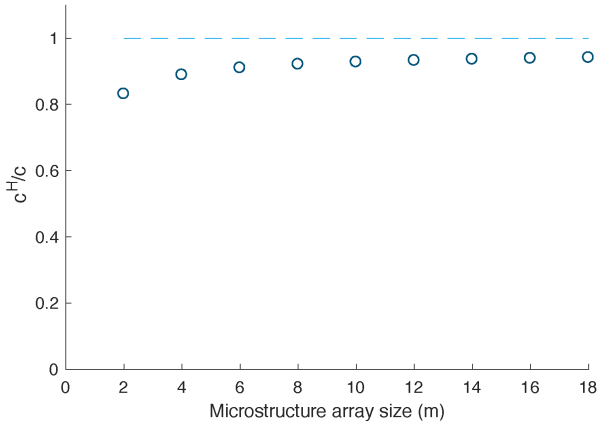

Figure 14: Normalized compliance vs. microstructural resolution.

Table 1: The structural compliance evaluated by homogenization and by full-scale analysis on the array of microstructures with and without consideration of compatibility.

	Homogenized	Full scale analysis
Individual formulation	2.436×10^2	1.899×10^8
Compound formulation	2.682×10^2	2.892×10^2

several orders of magnitude higher than predicted by numerical homogenization. In contrast, with the compound formulation ($\omega = 1$) the discrepancy is small.

4. Applicability to Multiscale Optimization

The proposed method for ensuring mechanical compatibility is also applicable to multiscale optimization. Rather than developing a new multiscale optimization framework, our intent here is to demonstrate the general applicability of the compound formulation for existing multiscale frameworks. In particular, we demonstrate it on a bottom-up approach [14] and a concurrent approach [19].

4.1. Bottom-up multiscale optimization

Following the method proposed by Cramer et al. [14], decoupled multiscale optimization is performed by first generating a family of microstructures optimized for maximum bulk modulus under linearly-varying volume constraint, and subsequently fitting their properties to a functional which then replaces the SIMP model (Eq. 8) in the macroscale optimization procedure.

This bottom-up approach is useful for some challenging loading conditions where density-based topology optimization methods do not converge to black-white solutions. Fig. 15 a) shows one such case. The beam is fixed at two ends, under a distributed load on the top and subject to a local volume constraint $\alpha = 60\%$. The density-based method [26] failed to produce binary structures and resulted in grey elements. Our method enables physically realizable microstructures to be mapped into such non-binary structures, shown in Fig. 15 b). Fig. 15 c) and

d) show alternative binary microstructures for comparison. In Fig. 15 c) the graded microstructures are generated by adapting the thickness of an 'X'-shaped unit. Parametrized lattices have been commonly used (e.g. [15, 16, 17]). In Fig. 15 d) the graded microstructures are optimized with a density filter across the unit cell domains to promote connectivity, following the approach proposed by Radman et al. [13]. Using full scale analysis, the compliance of the microstructures generated by our method is smaller than the other two, and is close to the compliance using homogenized properties.

The compound formulation generates families of microstructures which are compatible with their nearest neighbours on either side. In order to use the resulting microstructures in a bottom-up multiscale optimization procedure, the formulation has been modified to generate families of mutually compatible microstructures. In other words, each cell is compatible to any other cell in the family. The modified objective function for generating mutually compatible microstructures is:

$$\max_{\rho} \quad J = (1-\omega)\sum_{n=1}^{N} f(\overline{G}(\boldsymbol{\rho}^n)) + \omega \sum_{n=1,m>n}^{N} f(\overline{G}([\boldsymbol{\rho}^n, \boldsymbol{\rho}^m])). \tag{23}$$

As an example, Fig. 16 shows a sequence of microstructures generated with the original and modified compound formulation. In the latter case, non-adjacent microstructures possess improved compatibility with one another. The effects of the mutual compatibility are also shown in Fig. 5 e) for comparison to other options. This formulation increases the number of compound pairs from $N-1$ to $\frac{N(N-1)}{2}$, and can impede convergence.

The elasticity tensor for linearly-varying volume constraint is fitted by a functional which replaces the SIMP model. The functional takes the form:

$$G_{ij}^{fit}(\rho) = G_{ij}^{0}\Big(1 - \frac{1-\rho}{1+a_{ij}\rho}\Big), \tag{24}$$

where G_{ij}^{0} corresponds to a fully solid microstructure, and a_{ij} is the fitted coefficient. The functional matches the data very closely, and has the appropriate boundary values, i.e., $G_{ij}^{fit}(0) = 0$ and $G_{ij}^{fit}(1) = G_{ij}^{0}$ (see Fig. 17).

An isotropy constraint is imposed to ensure that the entries of the effective elasticity matrices vary monotonically with the average material density. Moreover, it reduces the number of parameters required to build the stiffness matrix from 6 (2D) or 21 (3D) to 2. This restriction reduces the computational cost of the optimization procedure, particularly for 3D implementations.

4.2. Concurrent multiscale optimization

In previous sections, the compound formulation has been applied to the design of structures with a finite number of unique microstructures. This formulation can also be adapted for use in concurrent multiscale optimization procedures, which typically

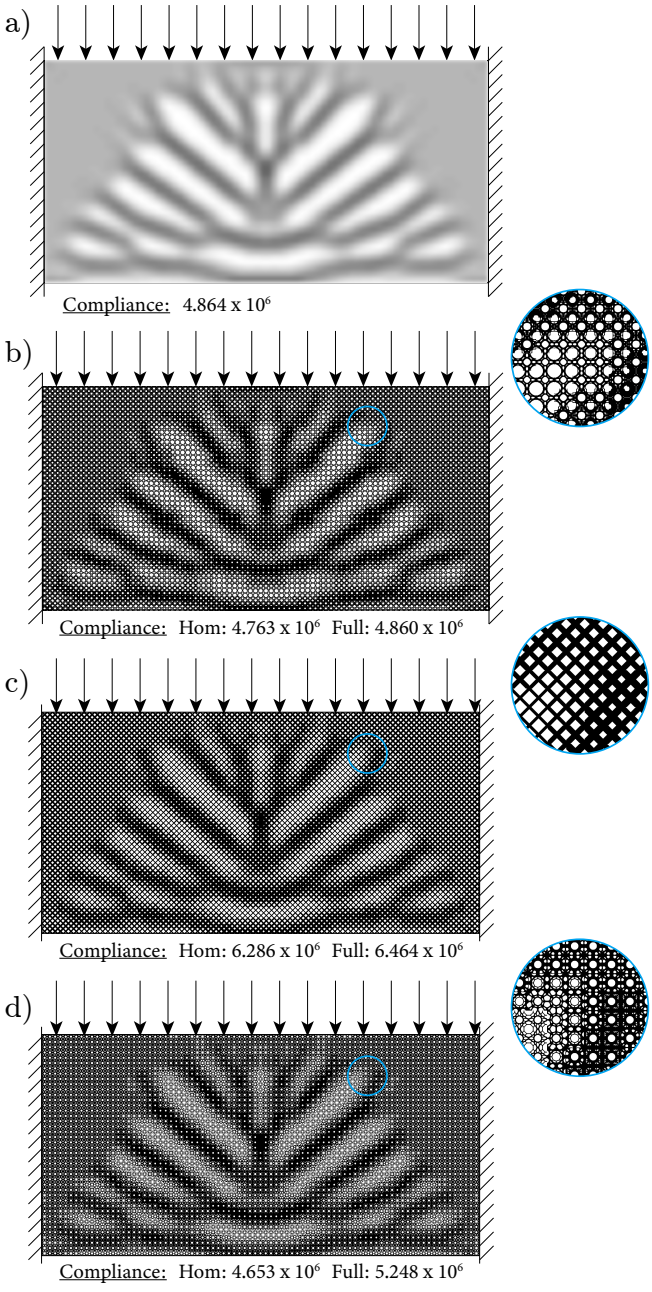

Figure 15: a) Non-convergent fixed beam under distributed load and subject to local volume fraction $\alpha = 60\%$. The binary structure can be realized by mapping b) compatible microstructures optimized by our method, c) 'X'-shaped lattices with varying thickness, and d) microstructures optimized by a density filter across the unit cell domains. For the binary structures, the compliances evaluated by homogenized properties (Hom) and by full scale analysis (Full) are reported.

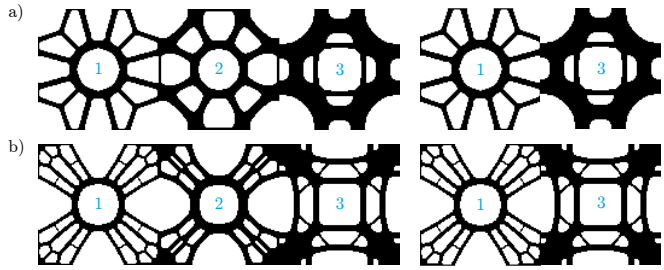

Figure 16: Sequence of microstructures generated: a) with compound formulation (Eq. 1), b) with modified compound formulation considering mutual compatibility (Eq. 23).

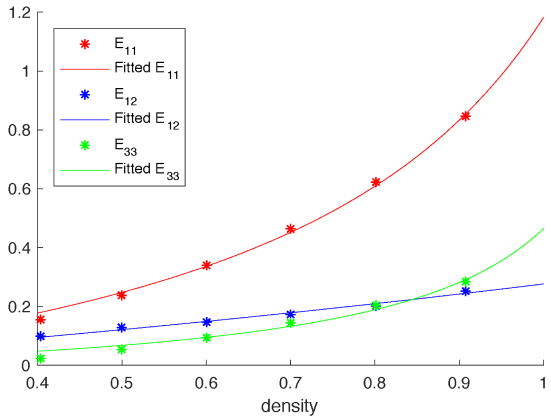

Figure 17: Fitted material property interpolation functions.

result in an unlimited number of microstructures. We follow the hierarchical concurrent material and structure scheme proposed by Rodrigues et al. [19]. In line with the compound formulation, we update the homogenized macroscale element stiffness tensor to be a weighted average of the element itself and a *superelement*, defined as the 3×3 (in 2D) Moore neighbourhood centred about the element, i.e.,

$$G_{ij}^{nm} = (1-\omega)G_{ij}^{nm} + \omega G_{ij}^{n\pm1,m\pm1} \tag{25}$$

where n and m are the macro level element coordinates. Fig. 18 shows a simply supported beam with 45×24 macro-elements and 60×60 micro-elements, subject to a 30% material constraint, optimized for minimum compliance using the concurrent multiscale scheme with and without the compound formulation. The boundary conditions are depicted in Fig. 18. The results show improved connectivity between adjacent microstructures and smoother topological gradation across the macrostructure. Furthermore, from multiple numerical tests it was observed that with the compound formulation the results are less dependent on the initialization of the design variables. Using full scale analysis it was observed that the improved connectivity reduces the compliance by more than four orders of magnitude. We note, however, that the compound formulation increases the homogenization-based compliance of the optimized structure by 28.8%. This could be explained by some distortion of the microstructures for ensuring compatibility. Moreover, even with improved connectivity there is a large discrepancy between the homogenization-based predictions and the results by full scale analysis.

5. Conclusions

In this paper, we have presented a novel method to ensure mechanical compatibility among topology optimized microstructures. By optimizing the mechanical properties of the compound cells, together with the properties of the individual cells, our method generates microstructures that form an integral part. Our results show that the bulk moduli of individual cells reach the theoretical bounds predicted by the Hashin-Shtrikman model, meaning that the optimization of compatibility does not compromise the performance of individual cells. Furthermore, the bulk moduli of neighbouring pairs also agree well with the Hashin-Shtrikman bounds. The method has been extended to allow maximum length scale and isotropy in microstructures. In a number of designs, including functionally graded materials and multiscale structures, we have demonstrated the effectiveness of the proposed method. The optimized microstructures can be fabricated by additive manufacturing technologies.

As future work, we are particularly interested in the following aspects. Firstly, this method is directly applicable to 3D design problems. To alleviate the computational burden in 3D, the GPU-based topology optimization framework [29] can be used. Secondly, while we have applied the compound formulation for maximizing bulk modulus, its applicability to other physical problems such as conductivity [40] is left to be demonstrated.

Acknowledgements

The authors wish to thank Krister Svanberg for sharing his Matlab implementation of the method of moving asymptotes (MMA).

References

[1] G. H. Loh, E. Pei, D. Harrison, M. D. Monzn, An overview of functionally graded additive manufacturing, Additive Manufacturing 23 (2018) 34 – 44. doi:10.1016/j.addma.2018.06.023.

[2] M. Osanov, J. K. Guest, Topology optimization for architected materials design, Annual Review of Materials Research 46 (1) (2016) 211–233. doi:10.1146/annurev-matsci-070115-031826.

[3] A. A. Zadpoor, Mechanical meta-materials, Materials Horizons 3 (2016) 371–381. doi:10.1039/C6MH00065G.

[4] M. Bendsøe, O. Sigmund, Topology Optimization: Theory, Methods, and Applications, Springer Berlin Heidelberg, 2011.

[5] O. Sigmund, Materials with prescribed constitutive parameters: An inverse homogenization problem, International Journal of Solids and Structures 31 (17) (1994) 2313 – 2329. doi:10.1016/0020-7683(94)90154-6.

[6] V. Challis, A. Roberts, A. Wilkins, Design of three dimensional isotropic microstructures for maximized stiffness and conductivity, International Journal of Solids and Structures 45 (14) (2008) 4130 – 4146. doi:10.1016/j.ijsolstr.2008.02.025.

[7] E. Andreassen, B. S. Lazarov, O. Sigmund, Design of manufacturable 3d extremal elastic microstructure, Mechanics of Materials 69 (1) (2014) 1 – 10. doi:10.1016/j.mechmat.2013.09.018.

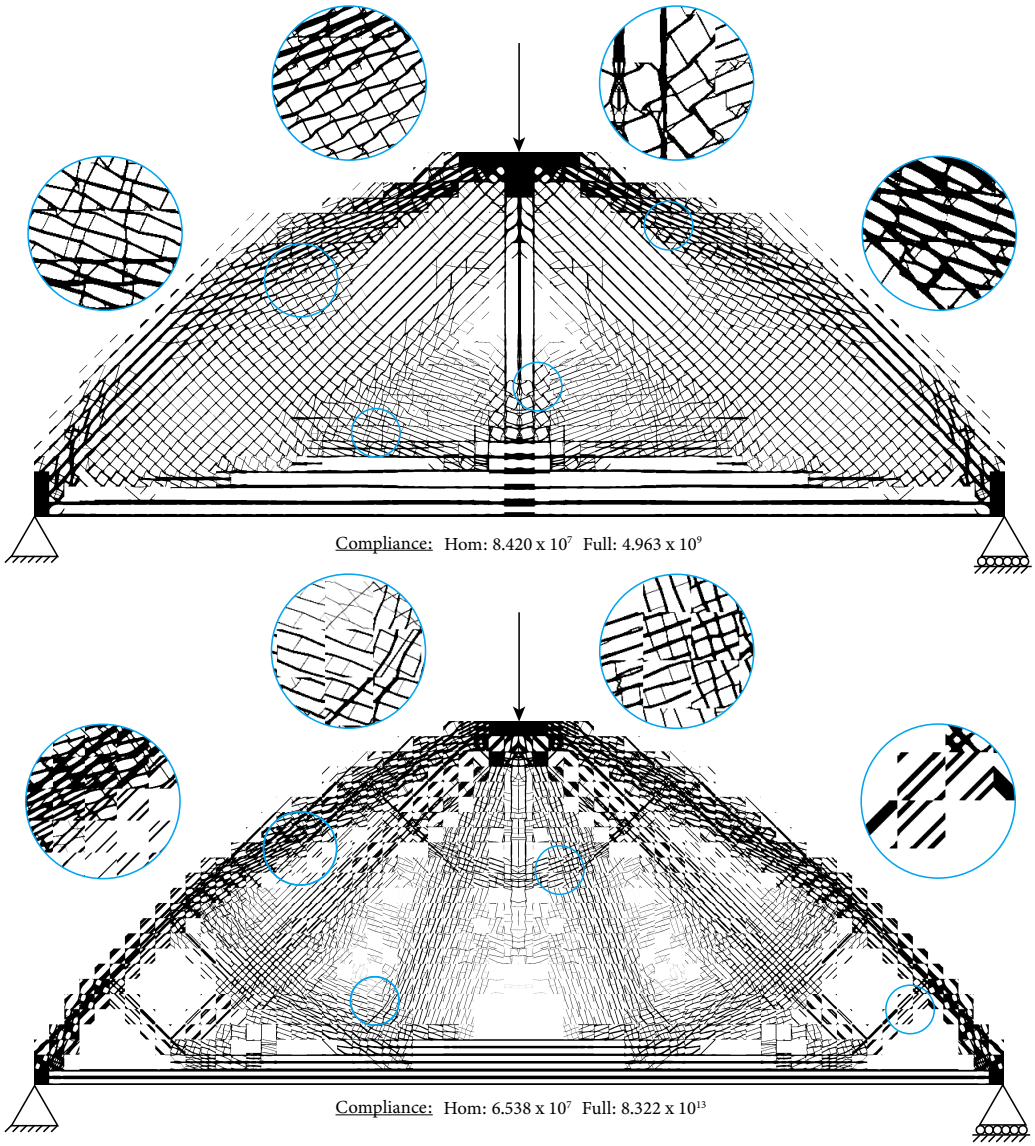

Figure 18: Multiscale optimization of a simply supported beam subject to 30% volume constraint with $\omega = 0.9$ (top) and $\omega = 0.0$ (bottom). The compliance is evaluated using homogenized properties (Hom) and full scale analysis (Full). Better connectivity of microstructures and lower compliance (using full scale analysis) are observed in the top.

[8] O. Sigmund, S. Torquato, Design of materials with extreme thermal expansion using a three-phase topology optimization method, Journal of the Mechanics and Physics of Solids 45 (6) (1997) 1037 – 1067. doi:10.1016/S0022-5096(96)00114-7.

[9] J. E. Cadman, S. Zhou, Y. Chen, Q. Li, On design of multi-functional microstructural materials, Journal of Materials Science 48 (1) (2013) 51–66. doi:10.1007/s10853-012-6643-4.

[10] V. K. Balla, S. Bodhak, S. Bose, A. Bandyopadhyay, Porous tantalum structures for bone implants: Fabrication, mechanical and in vitro biological properties, Acta Biomaterialia 6 (8) (2010) 3349 – 3359. doi:10.1016/j.actbio.2010.01.046.

[11] S. Zhou, Q. Li, Design of graded two-phase microstructures for tailored elasticity gradients, Journal of Materials Science 43 (15) (2008) 5157. doi:10.1007/s10853-008-2722-y.

[12] H. Li, Z. Luo, L. Gao, P. Walker, Topology optimization for functionally graded cellular composites with metamaterials by level sets, Computer Methods in Applied Mechanics and Engineering 328 (2018) 340 – 364. doi:10.1016/j.cma.2017.09.008.

[13] A. Radman, X. Huang, Y. M. Xie, Topology optimization of functionally graded cellular materials, Journal of Materials Science 48 (4) (2013) 1503–1510. doi:10.1007/s10853-012-6905-1.

[14] A. D. Cramer, V. J. Challis, A. P. Roberts, Microstructure interpolation for macroscopic design, Structural and Multidisciplinary Optimization 53 (3) (2016) 489–500. doi:10.1007/s00158-015-1344-7.

[15] C. Wang, J. H. Zhu, W. H. Zhang, S. Y. Li, J. Kong, Concurrent topology optimization design of structures and non-uniform parameterized lattice microstructures, Structural and Multidisciplinary Optimization 58 (1) (2018) 35–50. doi:10.1007/s00158-018-2009-0.

[16] A. Panesar, M. Abdi, D. Hickman, I. Ashcroft, Strategies for functionally graded lattice structures derived using topology optimisation for additive manufacturing, Additive Manufacturing 19 (2018) 81 – 94. doi:10.1016/j.addma.2017.11.008.

[17] D. Li, W. Liao, N. Dai, G. Dong, Y. Tang, Y. M. Xie, Optimal design and modeling of gyroid-based functionally graded cellular structures for additive manufacturing, Computer-Aided Design 104 (2018) 87 – 99. doi:10.1016/j.cad.2018.06.003.

[18] B. Zhu, M. Skouras, D. Chen, W. Matusik, Two-scale topology optimization with microstructures, ACM Trans. Graph. 36 (5). doi:10.1145/3095815.

[19] H. Rodrigues, J. Guedes, M. Bendsøe, Hierarchical optimization of material and structure, Structural and Multidisciplinary Optimization 24 (1) (2002) 1–10. doi:10.1007/s00158-002-0209-z.

[20] P. G. Coelho, P. R. Fernandes, J. M. Guedes, H. C. Rodrigues, A hierarchical model for concurrent material and topology optimisation of three-dimensional structures, Structural and Multidisciplinary Optimization 35 (2) (2008) 107–115. doi:10.1007/s00158-007-0141-3.

[21] L. Xia, P. Breitkopf, Recent advances on topology optimization of multiscale nonlinear structures, Archives of Computational Methods in Engineering 24 (2) (2017) 227–249. doi:10.1007/s11831-016-9170-7.

[22] Y. Wang, F. Chen, M. Y. Wang, Concurrent design with connectable graded microstructures, Computer Methods in Applied Mechanics and Engineering 317 (2017) 84 – 101. doi:10.1016/j.cma.2016.12.007.

[23] Y. Wang, L. Zhang, S. Daynes, H. Zhang, S. Feih, M. Y. Wang, Design of graded lattice structure with optimized mesostructures for additive manufacturing, Materials & Design 142 (2018) 114 – 123. doi:10.1016/j.matdes.2018.01.011.

[24] Z. Du, H. A. Kim, Multiscale design considering microstructure connectivity, in: 2018 AIAA/ASCE/AHS/ASC Structures, Structural Dynamics, and Materials Conference, 2018, p. 1385. doi:10.2514/6.2018-1385.

[25] J. Alexandersen, B. S. Lazarov, Topology optimisation of manufacturable microstructural details without length scale separation using a spectral coarse basis preconditioner, Computer Methods in Applied Mechanics and Engineering 290 (2015) 156 – 182. doi:10.1016/j.cma.2015.02.028.

[26] J. Wu, N. Aage, R. Westermann, O. Sigmund, Infill optimization for additive manufacturing; approaching bone-like porous structures, IEEE Transactions on Visualization and Computer Graphics 24 (2) (2018) 1127–1140. doi:10.1109/TVCG.2017.2655523.

[27] J. Wu, A. Clausen, O. Sigmund, Minimum compliance topology optimization of shellinfill composites for additive manufacturing, Computer Methods in Applied Mechanics and Engineering 326 (2017) 358 – 375. doi:10.1016/j.cma.2017.08.018.

[28] M. P. Bendsøe, O. Sigmund, Material interpolation schemes in topology optimization, Archive of Applied Mechanics 69 (9) (1999) 635–654. doi:10.1007/s004190050248.

[29] J. Wu, C. Dick, R. Westermann, A system for high-resolution topology optimization, IEEE Transactions on Visualization and Computer Graphics 22 (3) (2016) 1195–1208. doi:10.1109/TVCG.2015.2502588.

[30] J. Guedes, N. Kikuchi, Preprocessing and postprocessing for materials based on the homogenization method with adaptive finite element methods, Computer Methods in Applied Mechanics and Engineering 83 (2) (1990) 143 – 198. doi:10.1016/0045-7825(90)90148-F.

[31] L. Xia, P. Breitkopf, Design of materials using topology optimization and energy-based homogenization approach in Matlab, Structural and Multidisciplinary Optimization 52 (6) (2015) 1229–1241. doi:10.1007/s00158-015-1294-0.

[32] Z. Hashin, Analysis of composite materials—a survey, Journal of Applied Mechanics 50 (3) (1983) 481–505. doi:10.1115/1.3167081.

[33] K. Svanberg, The method of moving asymptotes—A new method for structural optimization, International Journal for Numerical Methods in Engineering 24 (2) (1987) 359–373. doi:10.1002/nme.1620240207.

[34] J. K. Guest, J. H. Prvost, T. Belytschko, Achieving minimum length scale in topology optimization using nodal design variables and projection functions, International Journal for Numerical Methods in Engineering 61 (2) (2004) 238–254. doi:10.1002/nme.1064.

[35] O. Sigmund, Morphology-based black and white filters for topology optimization, Structural and Multidisciplinary Optimization 33 (4) (2007) 401–424. doi:10.1007/s00158-006-0087-x.

[36] S. Xu, Y. Cai, G. Cheng, Volume preserving nonlinear density filter based on heaviside functions, Structural and Multidisciplinary Optimization 41 (4) (2010) 495–505. doi:10.1007/s00158-009-0452-7.

[37] F. Wang, B. S. Lazarov, O. Sigmund, On projection methods, convergence and robust formulations in topology optimization, Structural and Multidisciplinary Optimization 43 (6) (2011) 767–784. doi:10.1007/s00158-010-0602-y.

[38] Z. Hashin, S. Shtrikman, A variational approach to the theory of the elastic behaviour of multiphase materials, Journal of the Mechanics and Physics of Solids 11 (2) (1963) 127 – 140. doi:10.1016/0022-5096(63)90060-7.

[39] O. Amir, N. Aage, B. S. Lazarov, On multigrid-CG for efficient topology optimization, Structural and Multidisciplinary Optimization 49 (5) (2014) 815–829. doi:10.1007/s00158-013-1015-5.

[40] S. Yan, F. Wang, O. Sigmund, On the non-optimality of tree structures for heat conduction, International Journal of Heat and Mass Transfer 122 (2018) 660 – 680. doi:10.1016/j.ijheatmasstransfer.2018.01.114.